A&A 419, 673–683 (2004)
DOI: 10.1051/0004-6361:20035846

Astronomy & Astrophysics

Is T Leonis a superoutbursting intermediate polar?

S. Vrielmann, J.-U. Ness, and J. H. M. M. Schmitt

Hamburger Sternwarte, Universität Hamburg, Gojenbergsweg 112, 21029 Hamburg
e-mail: [svrielmann, jness, jschmitt]@hs.uni-hamburg.de

Received 11 December 2003 / Accepted 13 February 2004

Abstract. We present an *XMM-Newton* analysis of the cataclysmic variable T Leo. The X-ray light curve shows sinusoidal variation on a period P_x equal to $0.89^{+0.14}_{-0.10}$ times the previously spectroscopically determined orbital period. Furthermore, we find a signal in the power spectrum at 414 s that could be attributed to the spin period of the white dwarf. If true, T Leo would be the first confirmed superoutbursting intermediate polar (IP). The *spin profile* is double-peaked with a peak separation of about 1/3 spin phases. This appears to be a typical feature for IPs with a small magnetic field and fast white dwarf rotation.
An alternative explanation is that the 414 s signal is a Quasi-periodic Oscillation (QPO) that is caused by mass transfer variation from the secondary, a bright region ("blob") rotating in the disc at a radius of approximately $9R_{\rm wd}$ or – more likely – a travelling wave close to the inner disc edge of a dwarf nova with a low field white dwarf.
The *XMM-Newton* RGS spectra reveal *double peaked emission* for the O VIII Ly α line. Scenarios in the IP and dwarf nova model are discussed (an emitting ring in the disc, bright X-ray spot on disc edge, or emitting accretion funnels), but the intermediate polar model is favoured. Supported is this idea by the finding that only the red peak appears to be shifted and the "blue" peak is compatible with the rest wavelength. The red peak thus is caused by emission from the northern accretion spot when it faces the observer. Instead, the peak at the rest wavelength is caused when the southern accretion funnel is visible just on the lower edge of the white dwarf – with the velocity of the accreting material being perpendicular to the line of sight.

Key words. stars: binaries: close – stars: novae, cataclysmic variables – stars: individual: T Leo – X-rays: stars – accretion, accretion discs

1. Introduction

Cataclysmic variables (CVs) are close, interacting binaries, consisting of a white dwarf receiving matter from its companion, usually – and so in our case – a main sequence star. In non-magnetic systems, the matter is transfered via an accretion disc, while, if the white dwarf has a significant magnetic field, the inner part of the disc is disrupted (intermediate polar) or the formation of a disc is prevented altogether (polar). In both cases the transfered material couples to the magnetic field lines before falling onto the white dwarf. CVs have been found to emit radiation across the whole electromagnetic spectrum, as various energy sources are present within the system.

This paper focuses on *XMM-Newton* X-ray observations of the dwarf nova T Leo, i.e., we are looking at high energy sources within the system. These are usually the boundary layer (e.g., Wood et al. 1995), a hot corona of the white dwarf (Mahasena & Osaki 1999), or accretion funnels and accretion spots on the surface of the white dwarf in magnetic systems (e.g., Schwarz et al. 2002).

T Leo is a very short period dwarf nova of SU UMa type showing superoutbursts (Slovak et al. 1987; Kato & Fujino 1987). With $P_{\rm orb}$ = 84 min (Shafter & Szkody 1984) the orbital period is in fact close to the period minimum of about 76 min (e.g., Thorstensen et al. 2002) and makes T Leo therefore particularly interesting. So far, T Leo was only studied twice in detail in X-rays, once in superoutburst (with *RXTE* by Howell et al. 1999) and once in quiescence (with *ASCA* by Szkody et al. 2001). Howell et al. detected T Leo only on one of five days during the outburst and on that day the X-ray emission was five times lower than during quiescence (compared with previous pointed *ROSAT* PSPC observations by van Teeseling et al. 1996; Richman 1996). The timing of the detection coincides with a re-brightening of the system.

It seems to be a typical behaviour of dwarf novae that hard (3–12.2 keV) X-rays are suppressed during outburst as McGowan et al. (2003) find also for SS Cyg. They suggest that this lack of hard X-rays, originating in an optically thin disc corona, is caused by radiation driven disc winds stripping the coronal layers from the disc during an outburst (Meyer & Meyer-Hofmeister 1994).

Szkody et al. (2001) find a variation on the orbital period for their quiescent *ASCA* X-ray data: just before upper conjunction of the white dwarf the system brightens slightly. Otherwise the X-ray emission appears constant.

In this study we investigate spectral properties and the variability in the *XMM-Newton* data of the quiescent T Leo in order to learn more about the source of the X-ray emission. Hereby,

Send offprint requests to: S. Vrielmann,
e-mail: svrielmann@hs.uni-hamburg.de

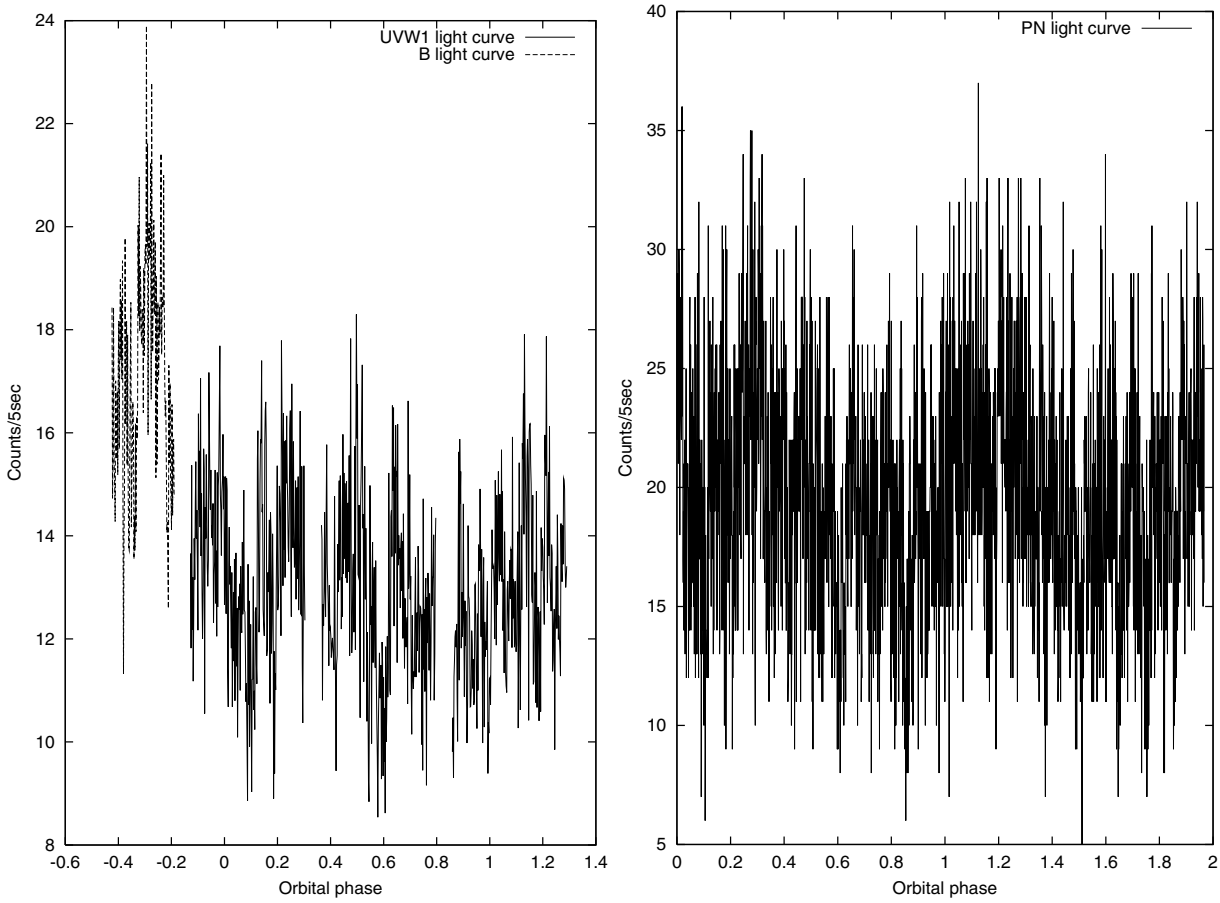

Fig. 1. OM (*B* and *UVW1*, *left*) and PN light curves at original resolution phased on the orbital period of 84 min. (Note, the data set is nearly exactly 2 orbital periods long, no repetition of data is plotted.)

two basic models are discussed to explain the behaviour of T Leo: the intermediate polar model, as previously suggested by Shafter & Szkody (1984) or the dwarf nova model as otherwise assumed (e.g., Kato 1997).

2. Data

The *XMM-Newton* data were taken on 1 June 2002 for a total of 11.4 ks during which all instruments were used, i.e., OM, EPIC (PN, MOS1, MOS2), and RGS. The OM data were taken in the *B* filter (duration 1.2 ks) and *UVW*1 filter (duration 7.2 ks). The effective wavelengths of the filters are 434 nm and 291 nm, respectively. The *B* filter data were taken prior to the RGS data, the *UVW*1 data mostly simultaneously with the X-ray data (see Table 1).

For the reduction we used the standard *SAS* software (version 5.4.1) without major problems, except for the OM data where we used the pipeline products. T Leo is weak enough in X-rays, so no measures had to be taken to work around pile-up.

3. Photometry

Figure 1 shows the light curves in the optical (*B* and *UVW*1 filter) and X-ray range phased on the orbital period $P_{\rm orb}$ = 1.41166 h determined through radial velocity curves in the wings of the Hα emission line (Shafter & Szkody 1984). The phasing of the light curve in Fig. 1 is arbitrary in that phase 0 is set to the start of the PN light curve.

Table 1. Observations log. All observations were taken on 1 June 2002.

Instrument	Data mode	Filter	Start UT	Stop UT
M1	Imaging	Medium	11:12:29	14:37:11
M2	Imaging	Thin1	11:12:43	14:37:12
OM	Imaging & Fast	*B*	11:09:57	11:29:57
OM	Imaging & Fast	*UVW*1	11:35:02	12:11:43
OM	Imaging & Fast	*UVW*1	12:16:49	12:53:29
OM	Imaging & Fast	*UVW*1	12:58:37	13:35:16
PN	Imaging	Medium	11:45:48	14:32:28
R1	Spectroscopy		11:06:11	14:40:37
R2	Spectroscopy		11:06:11	14:40:36

The light curves display strong flickering hidden in a high noise level as well as a strong variation dissimilar to that found by Szkody et al. (2001). While their light curves brighten only for 20% of the orbit, our light curves show rather sinusoidal or saw tooth like variation.

An FFT analysis does, unfortunately, not help in identifying, whether the variation is linked to $P_{\rm orb}$, as the length of the data set of approximately 2 $P_{\rm orb}$ gives us a very poor resolution

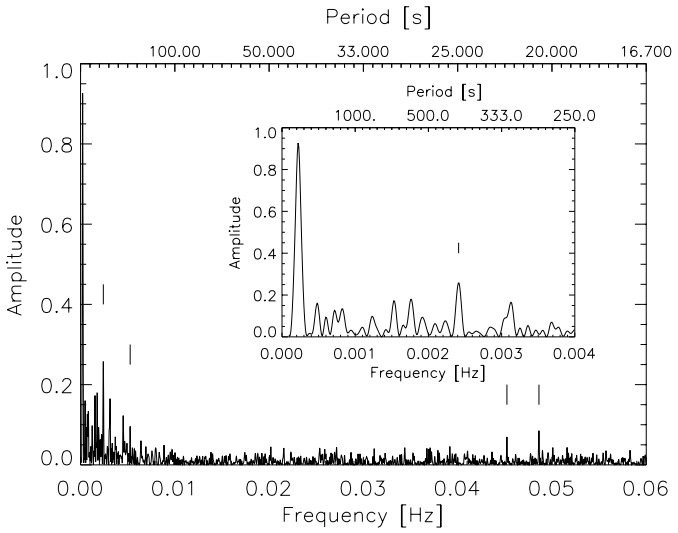

Fig. 2. Power spectrum of the PN light curve. The inset is a blow up of the low frequency range. The peak at low frequencies (at frequency 2×10^{-4} Hz) is consistent with the orbital period, however, allows a range of 1–1.6 h. The frequency range covers 3 h (length of data set) to 16 s. The vertical dashes denote the frequencies cited in the text, with periods (left to right) 414.42 s, 190 s, 22.112 s, 20.567 s. In the inset only the 414.42 s peak is marked.

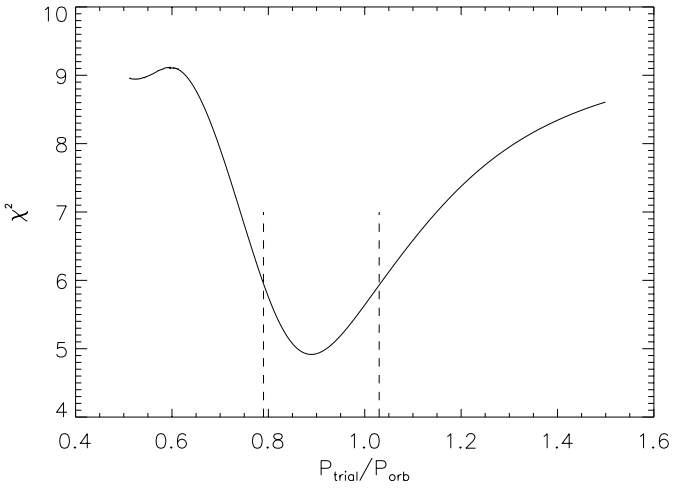

Fig. 3. The trial period in relation to the orbital period vs. the χ^2 of the sinusoidal fit. The minimum of the χ^2 lies at a period of $0.89P_{\rm orb}$. The dashed lines indicate the 1-σ error range.

in the power spectrum around $P_{\rm orb}$ (Fig. 2). The width of the peak around $P_{\rm orb}$ allows values between 1 h and 1.6 h.

Apart from the orbital peak we can identify a peak in the power spectrum at $(2.413 \pm 0.04) \times 10^{-3}$ Hz (=414 ± 7 s) and its overtones $(2f, 3f, 4f, 5f)$. This could be the spin period of the white dwarf or a Quasi-periodic oscillation (QPO). Furthermore, we would like to draw attention to the two minor peaks at 0.049 and 0.045 Hz (20.6 s and 22.1 s). The discussion of these peaks will follow in Sect. 5.1.2.

In order to check how stable the peaks are, we split up the PN light curve into two sets of equal length and analysed both independent sets individually. The 414 s peak appears in both power spectra. The power spectrum of the first half of the PN light curve shows a strong series of peaks of base $f = 1.53 \times$ 10−3 Hz (654 s) and its overtones $(2f, 3f, 5f, 6f$, but not $4f)$. The first three peaks (counting from the lowest frequency) in this series are even stronger than the 414 s peak. In the second power spectrum this signal is completely absent.

The only identical peaks in both power spectra are at the above mentioned peaks at 0.049 Hz (slightly stronger in the first power spectrum) and 0.045 Hz (slightly stronger in the second one) and one futher peak at at 5.26×10^{-3} Hz (190 s).

As a further method to analyse the significance of the peaks in the power spectrum we used a bootstrapping technique to estimate the statistical strength of random peaks. Therefore, we randomized the PN light curve and calculated the power spectrum. In 1000 runs the maxium peak has a median strength of 0.08 and never reaches higher than 0.16. This means we have a 0.999 confidence level that the 414 s peak with a strength of 0.26 is real. For the other peaks, in particular the 21 s and 22 s peaks – with strengths of 0.085 and 0.07, respectively – the significance is questionable and is only supported by the fact that they appear in two independent data sets (first half and second half of the PN light curve).

Futhermore, we analysed the MOS1 and MOS2 light curve for any signals. Since the signal-to-noise level is much lower than in the PN light curve, only the orbital peak and the peak at the $5f$ overtone of the 414 s period are well above the significance level. However, while the 414 s and 190 s peaks are present (even if with low strengths), the two 21 s peaks are not.

To examine whether there is a significant orbital modulation in the data set, we binned the PN light curve to 50 bins and fitted sinusoids of a number of periods to the data set. Figure 3 shows the resulting reduced χ^2's of the best fitting sinusoid vs. the trial period. The minimum of the reduced χ^2 lies at $P_x = 0.89^{+0.14}_{-0.10} P_{\rm orb}$. While the minimum at P_x seems to be clearly shifted to 90% $P_{\rm orb}$, the orbital period lies within the 1-σ error range of P_x. The amplitude of the sinusoid is 0.41 ± 0.04 counts s^{-1} and the zero-line lies at 3.89 ± 0.02 counts s^{-1}.

In Fig. 4 we show the binned PN light curve together with the best sinusoidal fit. The same plot also shows the binned *UVW*1 light curve. While it is perfectly acceptable to fit the UV data with a constant count rate ($\chi^2 = 7.20$), an overlayed and scaled sinusoid (with amplitude 0.045 counts s^{-1} and zero line at 2.6 counts s^{-1}) suggests that the sinusoidal variation seen in X-rays *might* also be present at UV wavelengths ($\chi^2 = 7.06$).

It is noticeable that several of the "down" peaks in the PN and *UVW*1 light curves seem to coincide, while it is not the case for the "up" peaks. This *might* mean that the emitting flickering sources have little coherence between its X-ray and UV emission, but are localized close enough to be occasionally simultaneously eclipsed or absorbed by non-emitting material.

4. Spectroscopy

Using the three different sets of spectra (PN, MOS, and RGS) of various resolutions and sensitivities, we have a large data set to fit a spectral model using all data simultaneously. We used *xspec* to fit two $n_{\rm H}$-absorbed *raymond* spectra, following

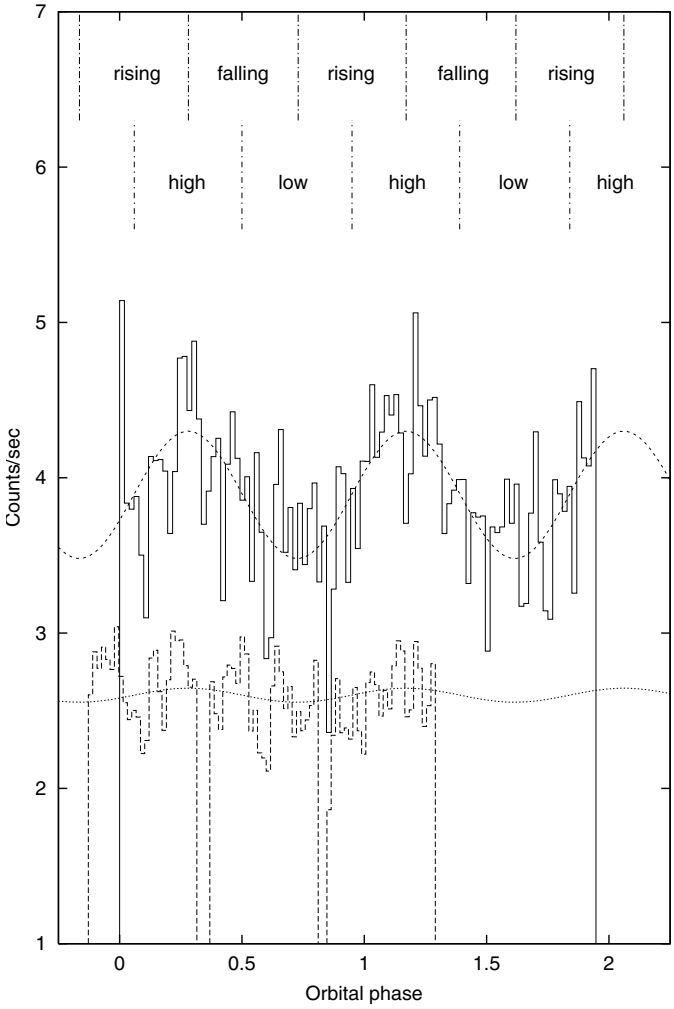

Fig. 4. Binned PN and OM (*UVW*1) light curves (solid and dashed histograms, respectively) with sinusoidal fit of period 0.89 $P_{\rm orb}$ to the PN data and a scaled sinusoidal function overlayed on the OM data. The labels above the light curves are for reference in the text (Sect. 5.2 and Fig. 11).

Table 2. Fitted parameters for simultaneous fit to MOS, PN, and RGS spectra.

Parameter	Value	Error	Unit
$n_{\rm H}$	0.132	0.072	10^{20} cm^{-2}
$kT_{\rm hot}$	4.06	0.06	keV
Norm$_{\rm hot}$	5.396	0.010	10^{-3}
$kT_{\rm cool}$	0.876	0.009	keV
Norm$_{\rm cool}$	0.240	0.041	10^{-3}

Units correspond to those in Szkody et al. (2001).

Szkody et al. (2001). The fitted parameters are given in Table 2. Figure 5 gives the spectra and fits for the PN and MOS data.

The fitted temperatures are similar to Szkody et al.'s, however, our column density is much smaller (by a factor of 10) and nearly vanishing, i.e., at the time of our observations the X-ray emitting gas was transparent. According to Howell et al. (1999) this column density is identical to that of the interstellar medium in the direction of T Leo (1.2 to 5×10^{19} cm^{-2}).

Table 3. Lines identified in RGS spectra. The entry "bad" means that the spectrum has a bad pixel at this wavelength (λ), "gap" means the line falls into the gap of the spectrum, "–" means the line was too faint to be measured. Other lines were too faint to determine a total flux.

Line	λ (Å)	Counts$_{\rm RGS1}$	Counts$_{\rm RGS2}$
Mg XII Ly α	8.42	23 ± 6	19 ± 6
Fe XXIII	10.98	*gap*	20 ± 6
Fe XVII	11.13	*gap*	23 ± 6
Ne X Ly α	12.13	*gap*	30 ± 8
Fe XVII	15.01	22 ± 6	–
O VIII Ly β	16.00	23 ± 6	12 ± 5
O VIII Ly α[1]	18.97	44 ± 14	41 ± 8
O VII	21.60	8 ± 4	*gap*
N VII	24.79	bad	14 ± 5
Ar XIV?	27.55[2]	–	10 ± 4

[1] Counts determined as sum of two Lorentzians fitted to the line profile (see Fig. 6).
[2] Blend of Ar XIV 27.47 Å and Ar XIV 27.63 Å.

In the RGS spectra we can identify a few lines as noted in Table 3. However, except for the O VIII Lyα line all lines are too noisy for an analysis of the line profile. The line fluxes (counts) were determined with the programme *CORA* (Ness & Wichmann 2002) using Lorentzian line profiles. The *FWHM* was in most cases fixed to 0.04 Å.

A more detailed look at the O VIII line (λ18.97 Å) reveals a double peaked structure (Fig. 6), similar to the emission lines O VIII, O VII, Ne X, and Ne IX in the Low Mass X-ray binary (LMXB) KZ TrA (4U 1626-67) (Schulz et al. 2001). The fitted Lorentzians have a separation of 950 km s^{-1} in both RGS1 and RGS2.

As the system (γ-) velocity of T Leo was determined to be 44 ± 20 km s^{-1} (Shafter & Szkody 1984) we can ignore it for our purposes, as the instrumental line broadening is already 0.04 Å (630 km s^{-1}).

In order to determine the significance of the double peaked structure of the O VIII line, we fitted the emission line with both single and double peaks to the line profile in the RGS1 spectrum. Hereby, the background was set to 25 counts/Å. A fit with instrumental profile with a width of 0.04 Å leads to a likelihood of $\mathcal{L} = -80.6$. In comparison, a single Gaussian with $\sigma = 0.042$ Å gives an $\mathcal{L} = -89.3$, a single Lorentzian of $FWHM = 0.12$ Å leads to $\mathcal{L} = -95.1$. Eventually, a fit of two Lorentzians of each $FWHM = 0.04$ Å gives even a significantly better likelihood of $\mathcal{L} = -96.5$ ($\Delta\mathcal{L} = 1.4$).

Schulz et al. (2001) explain the double peaked structure of emission lines in KZ Tra with emission from a narrow, highly ionized layer just above the optically thick disc surface and below an X-ray heated, fully ionized outer skin of an accretion disc. Such double peaked emission lines are typical for accretion discs with high inclination angles. However, the optical emission lines in T Leo are not clearly double peaked and the lack of eclipses points to an inclination angle no larger than 65° (Shafter & Szkody 1984; Szkody et al. 2001).

Inspecting Fig. 6 it is obvious that the positions of the O VIII line in the RGS1 and RGS2 spectra are not identical. While in the RGS1 the position of the *blue* peak is

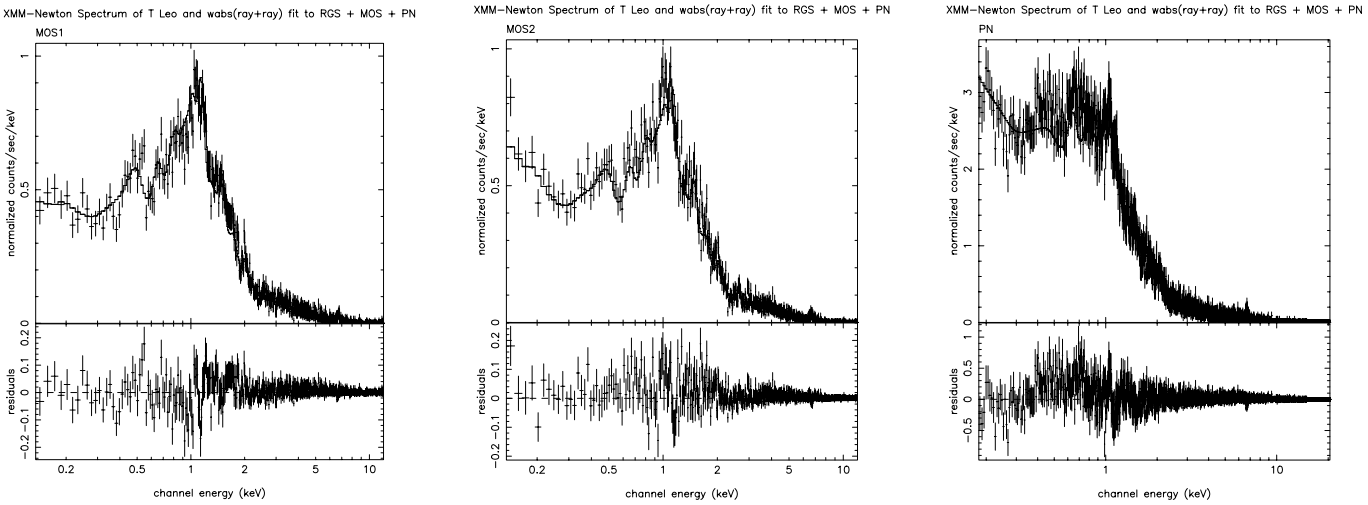

Fig. 5. EPIC MOS1, MOS2, and PN spectra with the simultaneous fit to the MOS, PN, and RGS data (χ^2 = 0.45). The comparison of the individual, observed spectra to the model spectra lead to χ^2's of the MOS1, MOS2, and PN of 0.73, 0.66, and 0.44, respectively.

compatible with the rest wavelength (λ18.96 Å ± 0.03 Å), the *red* peak is at 19.02 Å ± 0.03 Å (∼800 km s^{-1}). In the RGS2 spectrum the *blue* peak seams clearly shifted shortwards of the rest wavelength (λ18.94 Å±0.04 Å) while the *red* peak is marginally redder than the rest wavelength (λ19.00 Å±0.03 Å). We could exclude an error due to the positioning of the telescope using the catalogue position for extraction of the spectra. However, the positions of the red and blue peak in the RGS1 and RGS2 spectra are compatible with each other within the error range and lead to averages of $\lambda_{\rm blue}$ = 18.95 Å ± 0.03 Å and $\lambda_{\rm red}$ = 19.01 Å ± 0.02 Å. In particular, only the blue peak is compatible with the rest wavelength. It is however unclear, how the apparent line shift between the simultaneously taken RGS1 and RGS2 spectra is caused – if not by the low photon statistic.

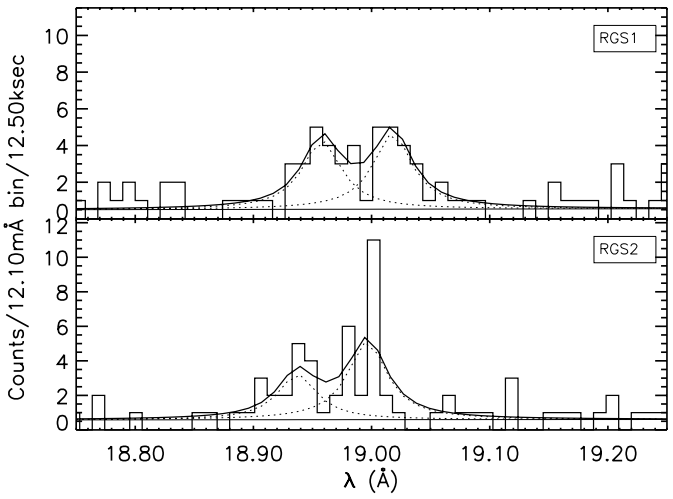

Fig. 6. Double peaked O VIII emission lines in the RGS1 (*top*) and the RGS2 (*bottom*) spectrum (histogram). The dotted lines in each plot are two Lorentzians (*FWHM* = 0.04 Å), the solid line the sum of the two Lorentzians. The *x*- and *y*-scales in both panels are identical.

The identification of the O VII line at 21.6 Å in the EPIC MOS1 spectrum allows us to estimate the temperature of the material where these two oxygen lines are formed from the O VIII/O VII line ratio. This yields a temperature range of (3 to 7) × 10^6 K using the errors in the total line counts. This temperature is somewhat lower than the temperature for the cool material found in the fit to all spectra of 10×10^6 K (see Table 2). However, another cool model component of a temperature as demanded from the O VIII/O VII line ratio would not significantly change the fit to the spectra (Fig. 5). Furthermore, we expect to find a distribution of temperatures in the accretion funnels and the accretion spots whereas the lower temperatures have much less significance in the spectral shape.

In the EPIC spectra we can identify a strong Fe XXV line complex. Fitting a single Lorentzian to this noisy line in the PN spectrum yields a total flux of (4.0 ± 2.1) × 10^{-5} photons cm^{-2} s^{-1} (= (4.2 ± 2.2) × 10^{-14} erg cm^{-2} s^{-1}) above a rather shallow continuum (4.3 ± 3.6) × 10^{-5} photons keV^{-1} cm^{-2} s^{-1}.

5. Discussion

5.1. Origin of the photometric variation

We discuss the observed frequencies in the light curve in order to investigate the nature of the system T Leo.

In order to investigate if P_x is caused by a beat period with $P_{\rm orb}$, we search for a variation on a timescale of about half a day. For this purpose we examined *ASCA* data from 1998 (Szkody et al. 2001) that were taken over a period of about 20 h. Figure 7 shows that there might indeed be a sinusoidal variation on a period of P_y = 10.5 h. However, the sinusoid with an amplitude of 0.042 counts s^{-1} has only a marginally better χ^2 of 2.24 compared to a constant flux (χ^2 = 2.62) and the peak at ∼13 h might also be a flare.

However, apart from the fact that the period P_x has an error range that is large enough to include the orbital period, it would be difficult to explain it. Neither a warped disc model

Table 4. Discussed periods. All but the first period refer to T Leo.

Symbol	Value	Explanation
$P_{\rm min}$	~76 min	Observed period minimum for Cataclysmic variables (e.g. Thorstensen et al. 2002).
$P_{\rm orb}$	84.69936 ± 0.00068 min	Orbital period (Shafter & Szkody 1984) determined from radial velocity measurements of Hα.
$P_{\rm sh}$	86.7 ± 0.1 min	Super hump period (Lemm et al. 1993).
P_x	75^{+12}_{-8} min	$0.89^{+0.14}_{-0.10} P_{\rm orb}$ as determined from our EPIC PN data, see Fig. 3.
P_y	10.5 h	Determined from *ASCA* data, see Fig. 7.
$P_{\rm spin}$	414 s	Spin period of white dwarf(?), see Fig. 2.

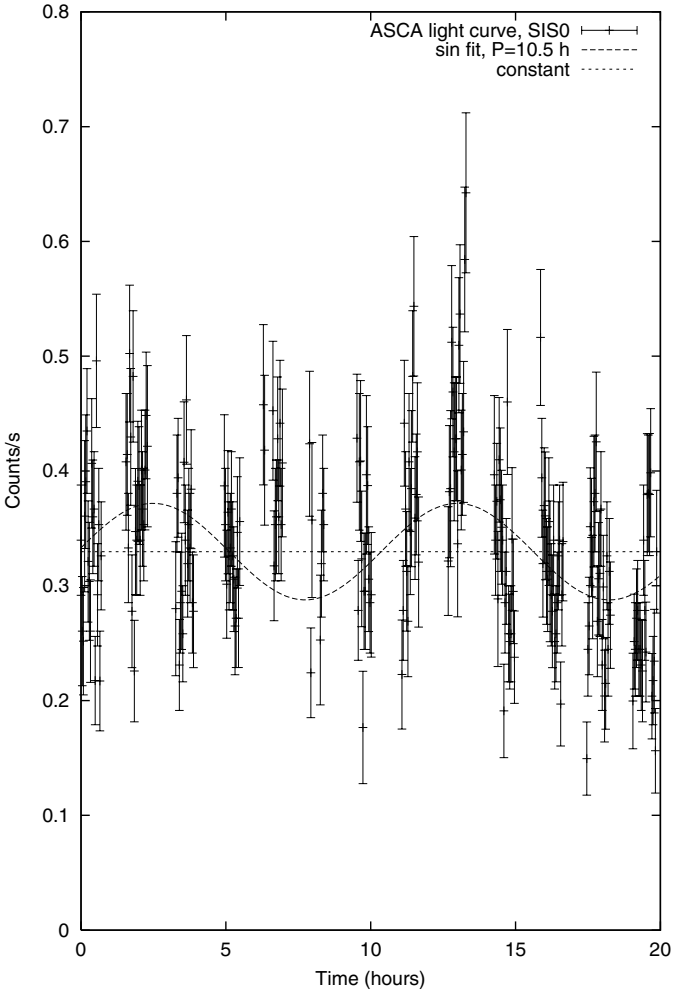

Fig. 7. *ASCA* SIS0 light curve with overplotted sinusoidal fit of period 10.5 h.

(e.g., Patterson 1999) nor a jet model (Livio 1998) can explain the periods P_x or P_y reasonably well or can be seriously considered. A sudden and extreme decrease of the orbital period in the last couple of decades can also be excluded (Kolb 2003, private communication). Therefore, we consider P_x to be identical to $P_{\rm orb}$. For clarity we collected the definitions of all discussed periods in Table 4.

In the next two Sections we discuss two models that could explain the observed period at 414 s: T Leo is either an intermediate polar or a dwarf nova showing Quasi-Periodic Oscillations.

5.1.1. Intermediate polar model

This scenario presumes that the white dwarf is slightly magnetic, just enough to disrupt the inner part of the disc up to no more than a few white dwarf radii (however, not to a complete absence of the disc, as (super) outbursts prove that a disc must be present). In such an intermediate polar (IP) the accreting material from the disc is forced to follow the magnetic field lines onto the two poles on the surface of the white dwarf. The X-ray emission then originates from the accretion column close to the white dwarf (e.g., King 1995).

Such a scenario was already proposed by Shafter & Skzody (1984). While the lack of optical polarisation can be easily explained with a weak magnetic field, it is more difficult to explain the lack of high excitation emission lines in the optical range. The lack of obvious orbital modulation in the optical and UV must then be related to a relatively low inclination angle of the system whose accretion disc mainly radiates at these long wavelengths. In contrast, the X-rays then originate to a large part from the accretion funnels and the accretion spots on the white dwarf which are much more prone to viewing angle changes than the disc, even in a low inclination system. It then seems likely that there is actually a small amount of variation visible in the UV as suggested in Fig. 4, because the accretion funnels will be hot and emit a bluer spectrum, thus be more pronounced in the UV than in the optical. However, in both the optical and UV the disc might be considerably brighter than the accretion funnel.

In IPs the magnetized white dwarf is usually desynchronized with a spin period of several hundred to thousand seconds. The peak in the power spectrum of the EPIC PN light curve at 414 s (Fig. 2) could thus indeed be interpreted as the spin period of the white dwarf. In Fig. 8 we plot the EPIC PN light curve folded onto the 414 s period. The simultaneous, independent EPIC MOS data are consistent with the spin profile, however, the shape is less pronounced due to much higher noise level. In particular, the MOS2 data show a better agreement with the PN data than the MOS1 data.

The spin profile is clearly double peaked with a peak-to-peak separation of about 0.3 to 0.4 (definitely <0.5) spin phases or roughly 1/3 of the orbit. Norton et al. (1999) observed a similar situation in the intermediate polar V709 Cas. However, while they see a peak in the power spectrum at a frequency $3/P_{\rm spin}$, our power spectrum does not show any obvious peak at this frequency ($3/P_{\rm spin} = 7.24 \times 10^{-3}$ Hz). On the other hand, considering the relative strength of the $1/P_{\rm spin}$ and $3/P_{\rm spin}$ peaks in Norton et al.'s power spectrum of about 5:1, a $3/P_{\rm spin}$

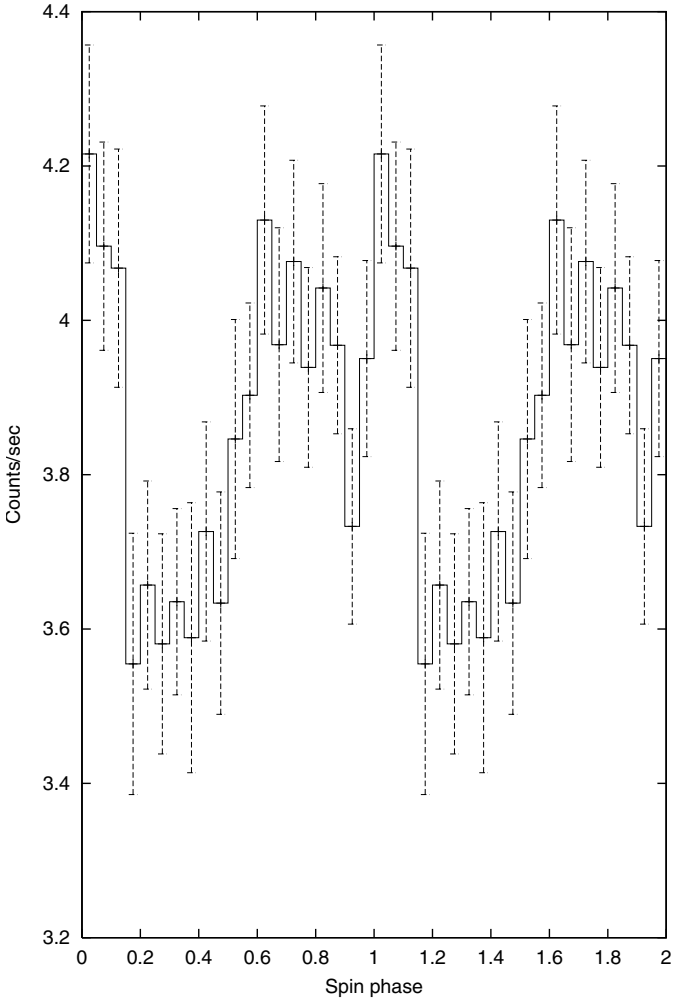

Fig. 8. The EPIC PN light curve folded on the period 0.1163 h = 414.42 s. The error bars are calculated from the scatter in the light curve. The light curve is plotted twice for clarity of the plot.

signal of an amplitude of the order 0.025 units might be hidden in the profile of another peak at 7.17×10^{-3} Hz (see Fig. 2).

A more detailed look reveals that in our case the full amplitude of the variation is only 10% of the signal (compared to 50% in V709 Cas). The system is brighter for about 2/3 of the orbit and shows a sharp drop after the second maximum. This *could* indicate a partial occultation of the X-ray source.

We do not find any significant signal at the beat frequency $(1/P_{\rm spin} - 1/P_{\rm orb})$, but possibly at $(1/P_{\rm spin} - n/P_{\rm orb})$ with $n = 5, 6$, and at $(1/P_{\rm spin} - 1/P_x)$ as well as $(1/P_{\rm spin} - n/P_x)$ with $n = 3, 4, 6, -1, -2, -3$. As Norton et al. (1999) point out, the beat frequency is usually a signal of stream-fed or disc overflow accretion and therefore more likely be observed in IPs with stronger magnetic fields. For T Leo this means it is one of the few systems that is disc-fed and seen at a relatively low angle. So far it is unclear what the observed frequencies represent, if they are significant.

In comparison to other IPs Norton et al. (1999) note that such double peaked profiles appear to arise particularly in white dwarfs with short spin periods (of less than about 700 s). This appears to be very well fulfilled. They argue further that the double peaked spin profile is caused by the small magnetic field (as we propose for T Leo's white dwarf). This either leads to large accretion areas and thus broad accretion curtains with optical depth reversal or (less likely because of the small inclination angle) accretion columns with conventional optical depth behaviour but that are tall enough to be partially visible from behind the white dwarf. In both scenarios the X-ray pulse maximum is seen whenever one of the poles is closest to the observer (see also Norton et al.'s Fig. 8). Since the maxima in the light curve folded on the spin period are less than 0.5 spin phases apart, the geometry of the magnetic field must be somewhat asymmetric.

All of this is most striking as the observed variations are only visible in X-rays, while at optical wavelengths no periodic signal has been observed (Shafter & Szkody 1984) and our UV data show only a very marginal periodicity if at all.

5.1.2. Dwarf nova model

An alternative model for T Leo is that it is a dwarf nova showing Quasi-periodic Oscillations (QPOs) and Dwarf Nova Oscillations (DNOs, for a review on QPOs and DNOs see Warner 2004). Dwarf novae show often short-lived QPOs with a period of a few hundred seconds. In DNO-related QPOs one can typically see DNOs with a period ratio $P_{\rm QPO}/P_{\rm DNO} \sim 15$. The frequencies around 21 s – if significant– could thus actually be the DNOs related to a 414 s QPO. As the nominal period deduced from the Keplerian velocity at the radius of the white dwarf is 16 s, it would mean that either the 20.567-s-signal arises from a disc annulus very close to the white dwarf or that the white dwarf has a high rotational velocity of 800 km s^{-1}.

A test for phase shifts between the first and second half of the data set does not help in deciding in favour of the QPO model as the measured phase shift of 0.1 is compatible with zero within the error range. Problematic for this model is, however, that the lightcurve folded on any of the two "DNO" periods reveals a double peaked curve instead of the expected highly sinusoidal signal (Fig. 9), although there might be exceptions (Warner 2004).

However, a number of dwarf novae have been found to show rapid oscillations in X-rays in quiescence usually of the order a few tens to a hundred seconds (Table 2 in Warner 2004). In particular, WZ Sge is the only one showing persistent DNOs and QPOs in quiescence (Warner & Woudt 2002).

The question arises, whether T Leo is similar to WZ Sge. T Leo certainly shows large amplitude outbursts, but is not generally considered a candidate for a WZ Sge type dwarf nova as it also shows normal outbursts (Kato et al. 2001). WZ Sge shows DNOs at 27.868 s and 28.952 s (mostly one of the two, but occasionally both simultaneously) and a period close to the beat period of the two DNOs at 742 s. These periods are explained as radiation from the central source with a rotation period of 27.868 s and a thickened region of the disc with a prograde rotation of period 744 s, the beat period of the DNOs, that reprocesses and obscures the radiation from the white dwarf (Warner & Woudt 2002).

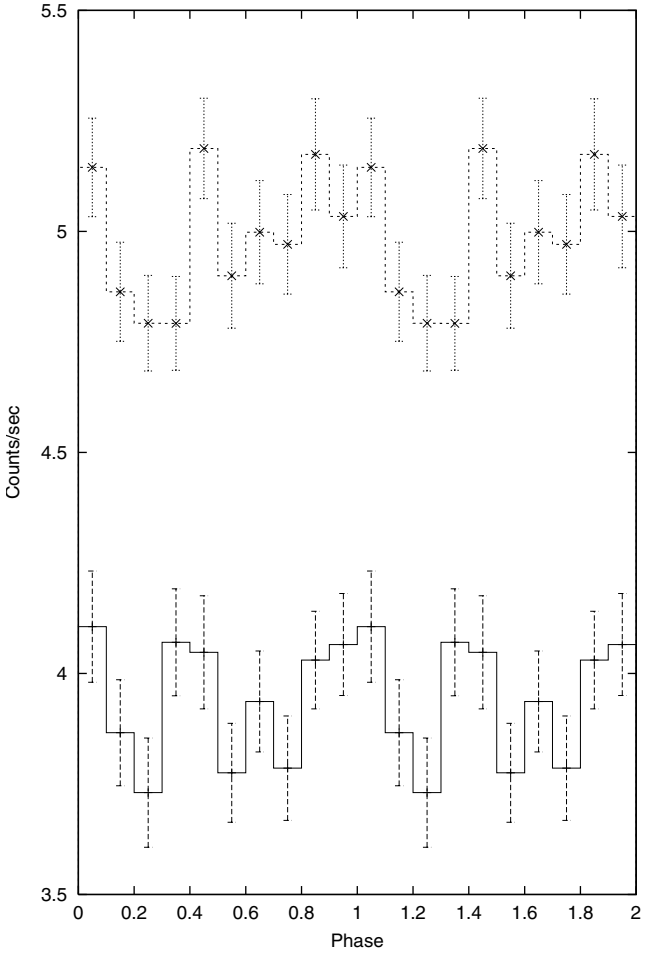

Fig. 9. The EPIC PN light curve folded on the period 20.567 s (*bottom*) and 22.112 s (*top*, shifted upwards by 1 counts s^{-1} for clarity of the plot).

In trying to apply this model to T Leo, we first notice that close to the expected beat period of the 20.567 s and 22.112 s periods (294 s) is only a minor peak with a maximum at 297 s in the power spectrum. We therefore dismiss the idea that T Leo displays DNO-related QPO and consider it likely that the frequencies around 21 s are not significant.

A more likely model, however, is that the QPOs in unrelated to any DNOs. One option is that the QPO is either caused by a modulated mass transfer rate through the inner Lagrangian point due to oscillations of the secondary similar to the 5-min oscillations on the sun (Warner 2004).

Another possibility is that the source of the variation is in the outer disc (Warner 2004). The period of 414 s corresponds to the Keplerian velocity of the disc material at a distance of $9R_{\rm wd}$. However, as T Leo is a SU UMa type dwarf nova and has therefore a rather large disc, this distance is likely at an intermediate radius, rather than at the disc edge (the 3:1 resonance radius $R_{3:1}$ is at $22R_{\rm wd}$, see Sect. 5.2.1 for system parameters).

We can better imagine a model in which a travelling front originates close to the inner disc edge of a slightly disrupted disc. In this scenario, proposed by Warner & Woudt (2002), the white dwarf has a low magnetic field, just large enough to disrupt the very inner part of the accretion disc. The stream from the secondary overflows the disc and impacts onto the inner disc edge. This can excite a buldge travelling retrogradely in the rotating disc (in fact a low frequency prograde $m = 1$ g-mode). Using Warner & Woudt's Eqs. 19 and 21 and the system parameters as described in Sect. 5.2.1, the impact radius is between 3.1 and 3.8 $R_{\rm wd}$ and the Keplerian period at this radius is between 160 s to 205 s (for mass ratios $q = 1/4$ to $1/6$). Thus, if the buldge is close to the disc edge it has a speed between a third to half the velocity of the disc material.

5.2. Origin of the emission line profile

The broadened, double peaked emission line we observe for O VIII could be caused by a) an accretion disc or ring, similarly to double peaked optical line emission in high inclination systems; b) a spot on the disc edge of an otherwise X-ray dark disc; in the dwarf nova model or c) accretion curtains in which the matter from the inner disc radius falls down onto a magnetic white dwarf, in the intermediate polar model.

In the following section we investigate which of these scenarios apply to T Leo.

5.2.1. Accretion disc or ring

The explanation that the O VIII emission arises in an accretion disc seems unlikely since the optical emission lines show only a very marginal double peaked structure (Shafter & Szkody 1984), particularly not as clear as the separation in the O VIII line. The inclination angle is with $i < 65°$ (Shafter & Szkody 1984; Szkody et al. 2001) too small to produce double peaks. It is, however, noticeable that the separation of the peaks in the O VIII line of ~950 km s^{-1}, i.e., ±475 km s^{-1}, fits to the velocities in the accretion disc in the Doppler Images of Shafter & Szkody.

It is, therefore, worth investigating if the emission in O VIII might be originating in a ring of narrow radial width in the disc. Simple model calculations can produce a double peaked U-shaped profile. While the model profiles have significant flux at the system velocity of the line, the observed profiles appear more clearly separated. However, due to the large noise in the data, we cannot exclude that the emission line profiles are produced in this way.

For a Keplerian ring in the accretion disc we can estimate the radius from the velocity $v \sin i$ and the white dwarf mass $M_{\rm wd}$. The system parameters of T Leo are quite uncertain, various values can be found in the literature. According to Shafter & Szkody (1984) the white dwarf has a mass $M_{\rm wd} < 0.4\ \mathcal{M}_\odot$ and an inclination angle $i < 65°$. This leads to an upper value for the ring radius of $0.31\ R_\odot \sim 31R_{\rm wd}$ (assuming $R_{\rm wd} = 0.01\ R_\odot$). The values derived by Belle et al. (1998) from model fitting of an IUE spectrum during an outburst of $M_{\rm wd} = 0.6\ \mathcal{M}_\odot$ and $i = 40°$ give a ring radius of $0.23\ R_\odot \sim 20R_{\rm wd}$ using their $R_{\rm wd}$ of 8×10^8 cm.

Using a secondary mass of $M_2 = 0.1\ \mathcal{M}_\odot$ (period-mass relation, Warner 1995) we obtain a mass ratio of $q = \frac{1}{4}$ or $\frac{1}{6}$, respectively. This leads to a distance from the white dwarf to the inner Lagrangian point L_1 in relation to the binary

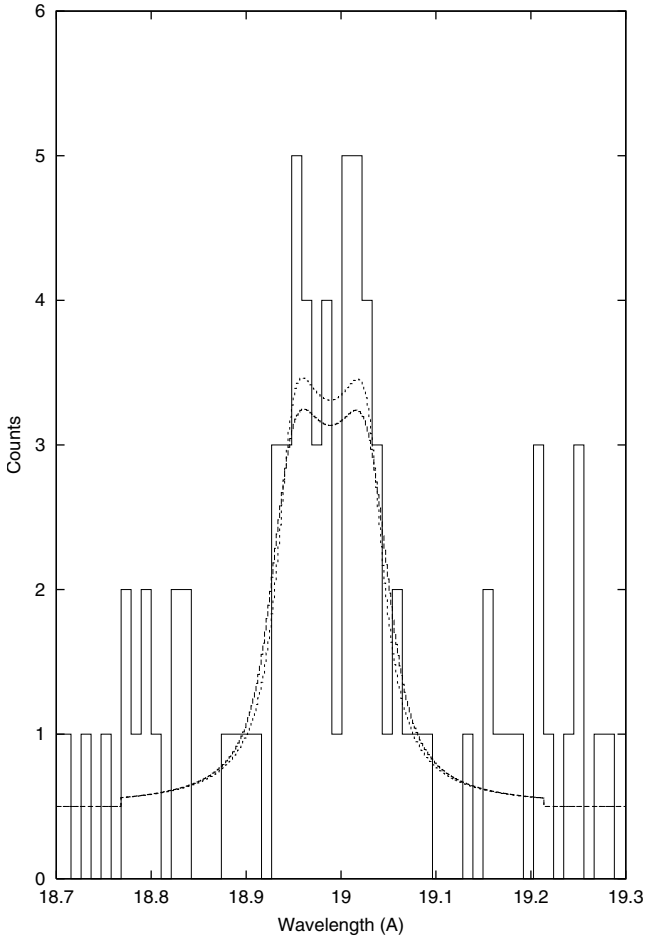

Fig. 10. O VIII emission line with overplotted models for an emitting ring in the accretion disc. The model profiles were convolved with a Lorentzian of 0.04 Å width. The ring is either narrow at a radius of $8R_{\rm wd}$ ($0.37R_{\rm L1}$, dashed line) or has a radius range between maximally $4R_{\rm wd}$ to $14R_{\rm wd}$ (0.18 to $0.65R_{\rm L1}$, dotted line). The normalization of the model profiles are chosen simply for illustrative purposes.

separation a of $R_{\rm L1}/a = 0.65 \pm 0.02$ (determined as the average of the $R_{\rm L1}/a$'s derived for the two values of q; Silber 1992; after Warner 1995). Using Warner's (1995) mass-radius relationship for the secondary gives a secondary radius of $R_2 \sim 0.136\ R_\odot$. With this we can derive the absolute distance from the white dwarf to the inner Lagrangian point $R_{\rm L1}$ to 0.25 $R_\odot$ or $22R_{\rm wd}$, i.e., for the following discussion we use Belle et al.'s (1998) system parameters as their parameters allows the proposed ring to be inside the Roche-lobe of the white dwarf. However, the true value must be somewhat larger, as the 3:1 resonance radius $R_{3:1}$ is at also $22R_{\rm wd}$, and during super outbursts the disc becomes larger than this. The true system parameters must therefore be slightly different from the quoted values.

As an example we constructed a simple model of an emitting ring and calculated the emission line profile folded with a Lorentzian with the observationally given resolution of 0.04 Å = 630 km s^{-1}. We could only achieve a double peaked profile with the peaks at the observed velocities (±475 km s^{-1}) and the observed line width for either a very narrow ring (<1%) at about $8R_{\rm wd}$ ($0.37R_{\rm L1}$) or a broader ring between maximal $4R_{\rm wd}$ and $14R_{\rm wd}$ (0.18 to $0.65R_{\rm L1}$) (Fig. 10). However, it is impossible to separate the two peaks clearly by assuming a ring structure.

This calculation shows that the ring model does not convincingly reproduce the observed results. Furthermore, the ring would have to be quite far from the hot inner disc (>$4R_{\rm wd}$) and it is unclear why only there the O VIII emission would be produced, as O VIII has a maximum at a temperature of 3×10^6 K. Such temperatures are only expected for the inner part of the disc (i.e., very close to the white dwarf).

In principle we can save this idea, if we assume that the disc is *warped* in the inner part of the disc. This would mean that the hot, inner disc has a different and variable inclination angle than the rest of the disc. This could explain the lack of correlation between the gradients in the light curve and the presence of double peaks as well as the single peaked optical emission lines. When we see it edge on, it becomes double peaked, however, at times when we face the inner part of the disc, the emission line becomes *narrow* not broad. However, this scenario is also problematic.

5.2.2. X-ray bright hot spot

In order to investigate option b), we compared the timings of the spectra with those of the X-ray light curve. Hereby, we assume that the sinusoidal variation in the PN light curve is caused by the bright spot moving in and out of view. Then we can separate the light curve in a *falling* portion, when the X-rays fade, and a *rising* portion, when the X-ray brighten according to Fig. 4. If the beaming hot spot theory is correct, we would expect that the spectra produced from timings of the *falling* portion of the light curve only show a red peak in the O VIII emission line, while the other spectra created from timings of the *rising* portions of the light curve should show only a blue peak. However, this is not the case (Fig. 11, left panel). While the "*blue*" spectrum clearly shows a double peaked structure for the O VIII line, the "*red*" spectrum simply shows a broadened emission line. Therefore, we have to dismiss this scenario. Interestingly, we find a correlation of the line strength with the high and low phases in the PN light curves (Fig. 11, right).

5.2.3. Accretion curtains in an Intermediate Polar

Eventually, we investigate, if (and how) the double peaked emission line can be produced within an IP model. This may include a scenario in which the white dwarf has a very low field as proposed for the QPO model (end of Sect. 5.1.2). This goes hand in hand with the question, if thus we should expect such *emission line profiles* for all IPs with small magnetic fields (and double peaked *spin profiles*).

In an IP the matter from the secondary is first fed into an accretion disc. This disc is disrupted at a certain inner radius from where the matter couples to the magnetic field lines of the white dwarf. This leads to accretion curtains through which the matter from the secondary is dumped onto the surface of the white dwarf.

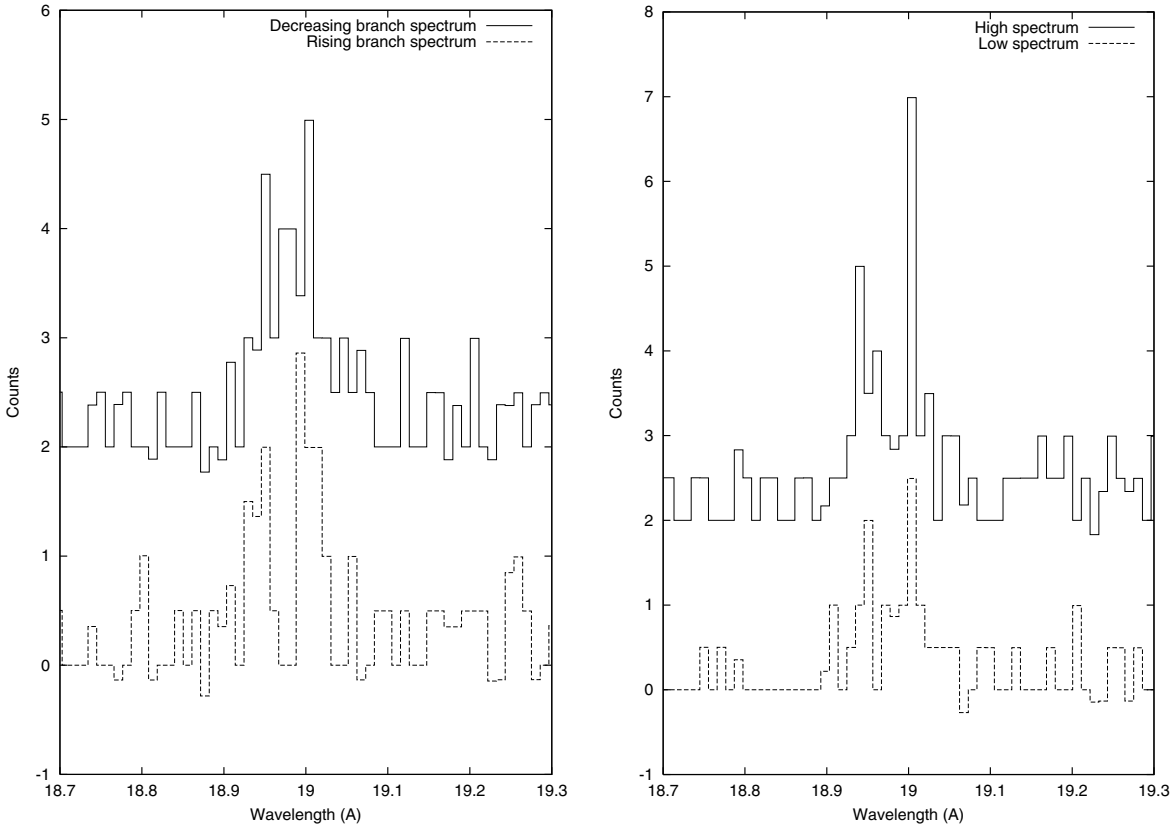

Fig. 11. Spectra during rising and falling (decreasing) phases (*left*) and spectra during high and low phases (*right*). The spectra for the decreasing branch phases and the high phases are shifted upwards by 2 counts for clarity of the plots. See Fig. 4 for identification of phase ranges.

Whenever the magnetic north pole (by definition the pole that is on the hemisphere closer to the observer) is facing the observer, the material in the accretion curtain is falling down onto the white dwarf, causing red shifted emission. However, at the timing of the second maximum the white dwarf has turned such that the material in the curtains moves perpendicular to the line of sight. Even if the accretion columns are tall enough so that the southern one is visible at the time of the first maximum from behind the white dwarf we would not expect blue-shifted emission, as the X-rays are produced too close to the white dwarf to be visible and the curtain bends too strongly to see any emitting material falling in the direction towards the observer.

We can expect both blue and redshifted emission, if the poles are moving in and out of view due to the rotation of the white dwarf. However, the rotational velocity of the white dwarf (using Belle et al.'s (1998) radius of 8×10^8 cm) is $2\pi R_{\rm wd}/P_{\rm spin} = 121$ km s^{-1}, much less than the observed ± 475 km s^{-1} in the emission line profile.

As mentioned in Sect. 4 emission line peaks are not shifted symmetrically to the rest wavelength, where the blue peak is compatible with the rest wavelength and the red one shifted to a positive velocity of about $v = +630 \pm 340$ km s^{-1}. This means, we see the red peak originating in the accretion funnel of the northern hemisphere in which the material is moving away from the observer onto the white dwarf (involving an optical depth reversal as proposed by Norton et al. 1999). The blue peak is not seen, as the infalling material with velocity towards the observer is hidden from the view behind the white dwarf. The peak at the rest wavelength comes from material moving perpendicular to the line of sight, e.g., at the phase when the southern pole is closest to the observer.

An analysis of spectra extracted during the phases of the two spin profile maxima and the single minimum (0.5−0.925, 0.925−1.15, 0.15−0.5, respectively, see Fig. 8) seems to support this idea (e.g. the emission during the broad maximum between spin phases 0.5 to 0.925 appears to show only the red peak), however, the count rates are too low to make any firm statements. Further observations with a more secure wavelength calibration and better S/N ratio are necessary to confirm this model.

The IP model for T Leo was first suggested by Shafter & Szkody (1984). In order to explain their measured radial velocity curve shift Warner (1995) proposes that the accretion stream from the secondary overflows the accretion disc and hits the inner disc edge similarly as in EX Hya. Shafter & Szkody's observed line width of Hα in fact is compatible with an inner disc radius of $6-7R_{\rm wd}$. However, as the disc is much cooler than the acretion funnels we do not expect any implication of the stream overflow model on our X-ray data.

T Leo is not the only suspect for an SU UMa type dwarf nova showing characteristics of an IP, however, it is the strongest candidate. SW UMa also shows superoutbursts with the typical features like superhumps (Robinson et al. 1987) and Shafter et al. (1986) discovered a period of 15.9 min that could be the rotation period of the magnetic white dwarf. However, Rosen et al. (1994) could not confirm the 15.9 min period with their data.

While the superoutbursting (Kato & Nogami 1997) VZ Pyx has been suspected to be an IP (de Martino et al. 1992; Remillard et al. 1994), Szkody & Silber (1996) point out, this system might not be an IP, as it shows coherent pulses only during decline from outburst. In contrast, our spin detection was made outside of any outburst. Furthermore, Warner et al. (2003) find QPO and DNO signals in their photometry of VZ Pyx, excluding the possibility that it is an IP. Another candidate is HT Cam (RX J0757.0+6306) which shows oscillations (Kemp et al. 2002), but whose SU UMa nature is not confirmed, yet (Tovmassian et al. 1998).

Further objects listed in Warner's (1995) Table 7.2 being SU UMa type dwarf nova and simultaneously IP candidates are AL Com and HT Cas. However, while both are clearly SU UMa stars showing super outbursts, there is no clear evidence that HT Cas is an IP (but possibly a VY Scl type object, Robertson & Honeycutt 1996), and AL Com shows only some properties similar to EX Hya (Abbott et al. 1992). All in all both are rather unusual objects, possibly linked to the WZ Sge-type dwarf novae.

6. Summary

The X-ray light curve reveals a period at 414 s that could be the spin period of the white dwarf $P_{\rm spin}$. Proven correct, this would make T Leo the first confirmed intermediate polar that displays superoutbursts. In this model it is relatively easy to explain the double peaked X-ray emission line O VIII (Ly α) originating in the accretion curtains. Furthermore, it would make T Leo extremely interesting, as it provides a unique opportunity to investigate the disc instability in a magnetic cataclysmic variable.

An alternative model is that the 414 s signal is a Quasi-periodic Oscillation, leaving T Leo to be a dwarf nova as usually assumed. These QPOs arise most likely in a mass transfer variation from the secondary or a distortion in the intermediate regions in the disc. However, it is very difficult – if not impossible – to explain the double peaked emission line O VIII (Ly α) in this model as the optical lines are single peaked.

It is, therefore, highly desirable to obtain further X-ray high resolution photometry and spectroscopy to investigate the stability of the 414 s signal and the shape of the X-ray emission line profiles. Only this will give us unambiguous answers concerning the nature of T Leonis.

Acknowledgements. This work is based on observations obtained with *XMM-Newton*, an ESA science mission with instruments and contributions directly funded by ESA Member States and the USA (NASA). S.V. and J.-U.N. acknowledge support from DLR under 50OR0105. Furthermore, we thank the referee for valuable comments leading to an improvement of the paper.

References

Abbott, T. M. C., Robinson, E. L., Hill, G. J., & Haswell, C. A. 1992, ApJ, 399, 680
Belle, K., Nguyen, Q., Fabian, D., Sion, E. M., & Huang, M. 1998, PASP, 110, 47
Homer, L., Anderson, S. F., Wachter, S., & Margon, B. 2002, AJ, 124, 3348
Howell, S. B., Ciardi, D. R., Szkody, P., et al. 1999, PASP, 111, 342
Kato, T. 1997, PASJ, 49, 583
Kato, T., & Fujino, S. 1987, Var. Star Bull. 3, 10
Kato, T., & Nogami, D. 1997, PASJ, 49, 481
Kato, T., Sekine, Y., & Hirata, R. 2001, PASJ, 53, 1191
Kato, T., Uemura, M., Ishioka, R., et al. 2004, PASJ, in press, [arXiv:astro-ph/0310209]
Kemp, J., Patterson, J., Thorstensen, J. R., et al. 2002, PASP, 114, 623
King, A. R. 1995, in Cape Workshop on magnetic cataclysmic variables, ed. D. A. H. Buckley, & B. Warner, ASP Conf. Ser., 85, 21
Lemm, K., Patterson, J., Thomas, G., & Skillman, D. R. 1993, PASP, 105, 1120
Livio, M. 1998, in Wild Stars In The Old West, Proc. of the 13th North American Workshop on CVs and Related Objects, ed. S. Howell, E. Kuulkers, & C. Woodward, ASP Conf. Ser., 137, 264
Mahasena, P., & Osaki, Y. 1999, PASJ, 51, 45
de Martino, D., Gonzalez-Riestra, R., Rodriguez, P., et al. 1992, IAUC, 5481
McGowan, K. E., Priedhorsky, W. C., & Trudolyubov, S. P. 2003, ApJ, in press
Meyer, F., Meyer-Hofmeister, E. 1994, A&A, 288, 175
Middleditch, J., Mason, K. O., Nelson, J. E., & White, N. E. 1981, ApJ, 244, 1001
Ness, J.-U., & Wichmann, R. 2002, AN, 323, 129
Norton, A. J. 2001, X-Ray astronomy: Stellar Endpoints, AGN, and the Diffuse X-ray Background, ed. N. E. White, G. Malaguti, & G. G. C. Palumbo, AIP Conf. Proc., 599, 806
Norton, A. J., Beadmore, A. P., Allan, A., & Hellier, C. 1999, A&A, 347, 203
Patterson, J. 1999, in Disk Instabilities in Close Binary Systems, Proc. of the Disk-Instability Workshop, 27–30 Oct. 1998, Kyoto, Japan, ed. S. Mineshige, & J. C. Wheeler (Universal Academy Press), Frontiers Sci. Ser., 26, 61
Remillard, R. A., Bradt, H. V., Brissenden, R. J. V., et al. 1994, ApJ, 428, 785
Richman, H. 1996, ApJ, 462, 404
Robertson, J. W., & Honeycutt, R. K. 1996, AJ, 112, 2248
Robinson, E. L., Shafter, A. W., Hill, J. A., Wood, M. A., & Mattei, J. A. 1987, ApJ, 313, 772
Rosen, S. R., Clayton, K. L., Osborne, J. P., & McGale, P. A. 1994, MNRAS, 269, 913
Schulz, N. S., Chakrabarty, D., Marshall, H. L., et al. 2001, ApJ, 563, 941
Schwarz, R., Greiner, J., Tovmassian, G. H., Zharikov, S. V., & Wenzel, W. 2002, A&A, 392, 505
Shafter, A. W., & Szkody, P. 1984, ApJ, 276, 305
Shafter, A. W., Szkody, P., & Thorstensen, J. R. 1986, ApJ, 308, 765
Slovak, M. H., Nelson, M. J., & Shafter, A. W. 1987, IAU Circ., 4314
Szkody, P., & Silber, A. 1996, AJ, 112, 289
Szkody, P., Nishikida, K., Long, K. S., & Fried, R. 2001, AJ, 121, 2761
Thorstensen, J. R., Patterson, J., Kemp, J., & Vennes, S. 2002, PASP, 114, 1108
Tovmassian, G. H., Greiner, J., Kroll, P., et al. 1998, A&A, 335, 227
van Teeseling, A., Beuermann, K., & Verbunt, F. 1996, A&A, 315, 467
Warner, B. 1995, Cataclysmic variable stars, Cambridge Astrophys. Ser. (Cambridge University Press), 207
Warner, B. 2004, PASP, invited review [arXiv:astro-ph/0312182]
Warner, B., & Woudt, P. A. 2002, MNRAS, 335, 84
Warner, B., Woudt, P. A., & Pretorius, M. L. 2003, MNRAS 344, 1193
Wood, J. H., Naylor, T., Hassall, B. J. M., & Ramseyer, T. F. 1995, MNRAS, 273, 772